PHILOSOPHICAL TRANSACTIONS OF THE ROYAL SOCIETY A MATHEMATICAL, PHYSICAL & ENGINEERING SCIENCES

# Bifurcations and Chaos in a Model of a Rolling Railway Wheelset

Carsten Knudsen, Rasmus Feldberg and Hans True

*Phil. Trans. R. Soc. Lond. A* 1992 **338**, 455-469
doi: 10.1098/rsta.1992.0014

# Bifurcations and chaos in a model of a rolling railway wheelset

By Carsten Knudsen[1,3], Rasmus Feldberg[1,3] and Hans True[2,3]

[1] *Physics Laboratory III*, [2] *Laboratory of Applied Mathematical Physics* and [3] *Center for Modelling, Nonlinear Dynamics and Irreversible Thermodynamics (MIDIT), The Technical University of Denmark, DK-2800 Lyngby, Denmark*

In this paper we present the results of a numerical investigation of the dynamics of a model of a suspended railway wheelset in the speed range between 0 and 180 km $h^{-1}$. The wheel rolls on a straight and horizontal track unaffected by external torques. A nonlinear relation between the creepage and the creep forces in the ideal wheel rail contact point is used. The effect of flange contact is modelled by a very stiff spring with a dead band. The suspension elements have linear characteristics, and the wheel profile is assumed to be conical. All other parameters than the speed are kept constant.

Both symmetric and asymmetric oscillations and chaotic motion are found. The results are presented as bifurcation diagrams, time series and Poincaré section plots. We apply bifurcation and path following routines to obtain the results.

In the last chapter we examine one of the chaotic regions with the help of symbolic dynamics.

## 1. Introduction

Railway vehicle dynamics is a fascinating topic in nonlinear mathematics and engineering. It is applicable to problems in the real world, and it is finite (although most often 'many') dimensional, so a solid foundation of mathematical theory exists and many methods are available to examine the problems. A variety of nonlinearities are imbedded in the problem formulations and therefore a variety of nonlinear effects are found in the results.

In this paper we examine a simple problem of motion. We consider a wheelset suspended under a moving car. No torques from motors or brakes act on the wheelset. It has been known since the early days of the railways that such a wheelset at higher velocities may oscillate in a lateral and yaw motion between the rails. This oscillation has a negative effect on riding comfort, and it increases the wear and therefore leads to higher maintenance costs. The phenomenon has therefore been the topic of several experimental and some theoretical investigations over the years.

The general situation is the following. Up to a certain speed the irregular motions of the vehicle will exclusively be a response to irregularities in the track geometry. Above a 'characteristic' speed, which for the same vehicle depends on external disturbances (e.g. track geometry or changes in the coefficient of friction), the vehicle will oscillate in the lateral and yaw direction. A linear stability analysis will most often yield a characteristic speed above the experimentally determined characteristic speeds, and much effort was spent trying to explain this fact. It was the nonlinear dynamical theory that finally yielded a satisfactory explanation.

*Phil. Trans. R. Soc. Lond.* A (1992) **338**, 455–469
*Printed in Great Britain*

The fundamental guidance system of railways consists of a flanged wheelset rolling on two rails. A clearance is provided between the outer edge of the flange and the inner face of the rail to prevent squeezing of the wheels between the rails. The cross section of the wheel tread is called the wheel profile. The angle between the tangent to the wheel profile and the centreline of the wheelset is most often positive. This makes the wheel kinematically self-centring.

If a disturbance pushes the wheelset laterally, the two wheels on the axle will roll on different radii. The difference in rolling radii will turn the wheelset and move it back towards its centred position. It is the cause of a kinematic instability, which was examined by Klingel (1883) in a celebrated paper. Since all dynamical forces were neglected, however, Klingel could not explain the discrepancies between the theoretically predicted critical speed and the experimental results.

The first work on the stability problem, where the dynamics was also included, was done by De Pater (1960). It was followed by papers by Matsudaira (1960) and Wickens (1965). These early works initiated a new wave of investigations around the world. We shall here only mention two articles, which are particularly relevant for this article, namely Cooperrider (1971) and the first bifurcation analysis of the problem by Huilgol (1978). For further references the reader is referred to the book edited by Kisilowski & Knothe (1991).

In this article we shall extend the investigation of the dynamical behaviour of the wheelset beyond the critical speed, where a Hopf bifurcation creates an auto-oscillation. The railway engineers call it 'hunting'. We treat the mathematical model as a parameter dependent dynamical system with the speed as the control parameter. It turns out that the system possesses a great variety of periodic and chaotic modes.

Kaas-Petersen (1986*a*) discovered chaos in railway dynamics. Meijaard & De Pater (1989) found chaos in the motion of a wheelset on a sineous track, and True (1989) continued Kaas-Petersens work. Jaschinski (1990) described chaotic behaviour of a bogie in his thesis and most recently Knudsen *et al.* (1991) found chaos in a model of a wheelset without flanges.

Chaos and bifurcations are the topics of several recent textbooks. In the context of the concepts, definitions and methods in this article we refer the reader to the books by Thompson & Stewart (1986) and Guckenheimer & Holmes (1983).

Our article is divided into six additional sections. In §2 the model is described. Section 3 contains the mathematical equations, and in §4 we explain how the problem is investigated. The results are presented in §5 and in connection herewith we analyse the supposed chaos in §6 with the use of symbolic dynamics in one of the speed intervals. Section 7 contains the conclusions.

## 2. The model

The mechanical problem to be considered is that of a guided wheelset under a car moving with constant speed along an ideal, rigid, straight and horizontal track. The speed $V$ is the control parameter in the problem. To illustrate a variety of possible motions we shall consider here a case close to the 'worst possible case' with no damping and no yaw stiffness.

The wheelset has two wheels rigidly connected with an axle. The wheels are frustums of a cone with slope $\lambda$. The wheels roll on rail surfaces, which are assumed to be an arc of a circle with radius $r_0$. The restoring force from the flanges on the

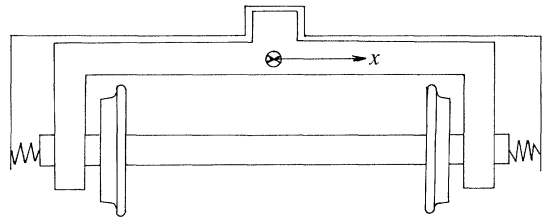


Figure 1. Arrangement of the wheelset with moving coordinate system.

wheels is approximated by a strong linear spring with a dead band and no damping. The wheelset can roll and move laterally without friction in a frame. The lateral motion is restricted by linear springs with no damping.

The frame can rotate around a frictionless vertical pivot, which is fixed in the car floor. The wheels, the axle, the frame and the car are all assumed to be rigid bodies. Figure 1 shows the arrangement of the wheelset.

The resultant of the normal forces exerted between the wheels and the rails generally has a lateral component. It vanishes in our model, because the wheel profile is conical.

Friction is only included in the contact forces between the wheels and the rail. When a loaded wheel rolls and simultaneously experiences a lateral or longitudinal force, tangential or shear stresses are generated in the contact zone between the elastic bodies. Under such rolling conditions the two bodies remain locked together over a portion of the contact region, as they would, if rolling took place without slip. However, slip does occur between the wheel and the rail in the remainder of the contact zone. This gives rise to a very complicated strain–stress relation in the contact surface.

Over the years simpler models of the strain–stress relation in the contact surface have been formulated. A common feature of these models is that they relate the resultant tangential force in the contact surface to the relative strain rate between the wheel and the rail in the ideal contact point. The ideal contact point can be calculated under the assumption that both wheel and rail are perfectly rigid. Under the assumptions made in our problem no more than one contact point exists on each wheel. The relative strain rate normalized by the forward speed of the car is termed the creepage. In general, the creepage consists of a part stemming from pure translational sliding (the translational creepage) and a part due to the yaw motion of the wheel, called the spin creepage.

The tangential forces in the contact surface, which will now be assumed to be a plane, may be projected in a direction parallel to the direction of wheelset travel, and in a direction orthogonal to it in the contact plane. The tangential force parallel to the direction of wheelset travel is called the longitudinal creep force, and the other component is called the lateral creep force.

The general form of the relation between the total creepage and the total creep force is similar to the one shown in figure 2. The function is nonlinear owing to the limitation of the forces imposed by the Coulomb friction law. The asymptotic limit corresponding to the Coulomb friction law is attained in the limit of pure sliding.

The creep forces are the main ingredients in railway vehicle dynamics. Since the theory yields a relation between the resultant creep force and the resultant creepage, the longitudinal creep force has a reciprocal effect on the lateral creep force. Furthermore the effect of spin creepage is to produce a lateral force. This contribution

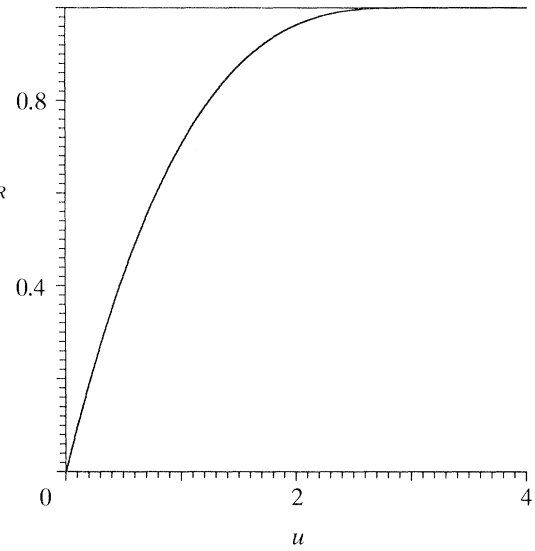


Figure 2. The creepage–creep-force relation by Vermeulen & Johnson (1964).

to the total lateral force reduces the longitudinal creep force; sometimes quite substantially, so altogether there exists a rather complicated relation between all the creepages and the components of the creep force.

It is now generally acknowledged that the most accurate creepage–creep-force relations have been formulated by Kalker. In his book, Kalker (1990) describes his results and compares them with other approximate solutions to the problem. To describe the bifurcation phenomena in the proper way we need here a fully nonlinear theory. Kalker's fully nonlinear theory is complicated, and its numerical handling is computationally expensive. We therefore use the formulas from Vermeulen & Johnson (1964) to calculate the creep forces. In their theory they neglect spin creep, but the saturation due to the Coulomb friction limit is taken into consideration. It thus contains the most important nonlinear effects that are necessary to describe the bifurcations. However, since spin creep is neglected we can only expect accurate results when the yaw of the wheelset is of small magnitude and flange contact does not occur.

Other theoretical results found by Knudsen *et al.* (1991) and G. Sauvage & J. P. Pascal (personal communication), who all use more accurate creep force models, show the same qualitative behaviour as our results. We therefore believe that our results are at least qualitatively correct in the case of flange contact, and are very accurate when the lateral displacements do not lead to flange contact.

When the flange of the wheelset touches the rail the restoring force suddenly grows much faster with the lateral displacement. The very stiff spring with a dead band in our model is just a simple simulation of that effect. There is very little doubt that it is that change in apparent or real stiffness that is the main cause of the chaotic behaviour of the wheelset. The results found will not depend qualitatively on the details of the model of the flange contact forces.

The wheelset has two degrees of freedom. It can turn around a central vertical axis and move laterally in its bearings. The equations of motion are formulated using Newton's second law on the solid wheelset under the action of the creep forces, the flange forces and the spring forces. The equations of motion are shown in the next




PHILOSOPHICAL TRANSACTIONS OF THE ROYAL SOCIETY A MATHEMATICAL, PHYSICAL & ENGINEERING SCIENCES

section together with the expressions for the creepage $\xi_R$ with the lateral component $\xi_x$, the longitudinal component $\xi_y$, and the creep force $F_R$ with the lateral component $F_x$ and the longitudinal component $F_y$.

## 3. Equations of motion

Under the assumptions of §2 the equations of motion are as follows:

$$\xi_x = \dot{x}/V - \phi, \tag{1}$$

$$\xi_y = a\dot{\phi}/V + \lambda x/r_0, \tag{2}$$

$$\xi_R = \sqrt{((\xi_x/\Psi)^2 + (\xi_y/\Phi)^2)}, \tag{3}$$

$$F_x = (\xi_x/\Psi)\, F_R/\xi_R, \tag{4}$$

$$F_y = (\xi_y/\Phi)\, F_R/\xi_R, \tag{5}$$

$$u = (G\pi a_e b_e/\mu N)\, \xi_R, \tag{6}$$

$$F_R = \mu N \begin{cases} u - \frac{1}{3}u^2 + \frac{1}{27}u^3, & u < 3, \\ 1, & u \geqslant 3, \end{cases} \tag{7}$$

$$F_T(x) = \begin{cases} k_0(x-\delta), & \delta < x, \\ 0, & -\delta \leqslant x \leqslant \delta, \\ k_0(x+\delta), & x < -\delta, \end{cases} \tag{8}$$

$$m\,\mathrm{d}^2x/\mathrm{d}t^2 + 2k_1 x + 2F_x + F_T(x) = 0, \tag{9}$$

$$I\,\mathrm{d}^2\phi/\mathrm{d}t^2 + 2k_2 d_1^2 \phi + 2aF_y = 0. \tag{10}$$

$x$ denotes the lateral displacement, and $\phi$ the yaw angle. In table 1 we explain the meaning of the other symbols and the values we have assigned to them in this article. $\Psi$ and $\Phi$ are coefficients calculated from Johnson's formula using Hertz contact theory.

## 4. The method of investigation

The mathematical model of our problem corresponds to a model of two coupled oscillators. The nonlinear creepage–creep-force relation in the wheel–rail contact points couples the two equations together.

We make the change of variables,

$$x_1 = x, \quad x_2 = \dot{x}, \quad x_3 = \phi, \quad x_4 = \dot{\phi}$$

(a dot above the variable denotes differentiation with respect to the independent variable, time), to obtain the following fourth-order autonomous dynamical system:

$$\dot{x}_1 = x_2, \tag{11}$$

$$\dot{x}_2 = -2(k_1/m)\, x_1 - (2/m)\, F_x - (1/m)\, F_T(x_1), \tag{12}$$

$$\dot{x}_3 = x_4, \tag{13}$$

$$\dot{x}_4 = -2(k_2 d_1^2/I)\, x_3 - 2(a/I)\, F_y. \tag{14}$$

The term containing $k_2$ is brought along for the sake of completeness, although $k_2 = 0$ in this article.

We want to illustrate the dynamics of the wheelset model through bifurcation diagrams with the speed $V$ as the control variable.

The problem is investigated numerically, and we use several methods that supplement each other to give the conclusions the best possible support.

Table 1

| constant | value | description |
|---|---|---|
| $m$ | 1022 kg | mass of wheelaxle |
| $I$ | 678 kg m$^2$ | moment of inertia |
| $a$ | 0.716 m | half of the track gauge |
| $d_1$ | 0.620 m | distance from centre of gravity to $k_2$ |
| $G$ | 808 MN m$^{-2}$ | shear modulus |
| $a_e$ | 6.578 mm | major semiaxis of contact ellipse |
| $b_e$ | 3.934 mm | minor semiaxis of contact ellipse |
| $\delta$ | 9.1 mm | dead band |
| $k_0$ | 14.60 MN m$^{-1}$ | spring constant |
| $k_1$ | $1.823 \times 10^4$ N m$^{-1}$ | spring constant |
| $k_2$ | 0 MN m$^{-1}$ | spring constant |
| $\Psi$ | 0.542 19 | — |
| $\Phi$ | 0.602 52 | — |
| $r_0$ | 0.457 2 m | centred wheel rolling radius |
| $\lambda$ | 0.05 | — |
| $\mu$ | 0.15 | coefficient of friction |
| $\mu N$ | 10 kN | $N$ is the vertical force between wheel and rail |

Our strategy is to start with a solution (the trivial solution) that is known to be asymptotically stable at sufficiently low speed. We then increase the speed in small steps and follow the solution and the eigenvalues of its jacobian by numerical solution of the system and numerical computation of the eigenvalues for each value of the speed. When a bifurcation point is reached, we choose the path to be followed in the phase-parameter space. When the increments in the control parameter are adequate, the known solution will provide an excellent initial value for the determination of the next solution on the path. The program 'PATH' is used for the investigations of the stationary and periodic solutions. The program was developed by Kaas-Petersen (1986*b*, 1989). Its most important feature is that it uses a mixture of integration in time and Newton iteration to find the periodic solutions, whereby the computational work is kept to a minimum. A periodic solution is treated as the identity under a Poincaré map. In this way the program determines stable and unstable solutions with the same accuracy. The Poincaré section is chosen by PATH in such a way that it is 'sufficiently transversal' to the phase space trajectory. In the chaotic régime we make both amplitude plots and Poincaré sections for different speeds. Here the Poincaré sections are defined by $x_2 = 0$ and $x_1$ assuming its maximum value. The amplitude plots are combined with the results from PATH to create our bifurcation diagrams. Furthermore a few interesting time series are shown.

For the numerical integrations we use either the 'LSODA' routine, which automatically switches between stiff and non-stiff solution methods whenever needed (see Petzold 1983) or an eighth-stage explicit Runge–Kutta pair of order five and six. It uses variable time step and error control. To approximate the solution between integration steps, we use an interpolant with asymptotic error of the same order as the global error for the numerical integration. The method was developed by Enright *et al.* (1986). The flange forces introduce a discontinuity in the first derivative of the lateral forces, but they remain continuous. We therefore use the two integration methods for any value of the lateral displacement of the wheelset.

Figure 3

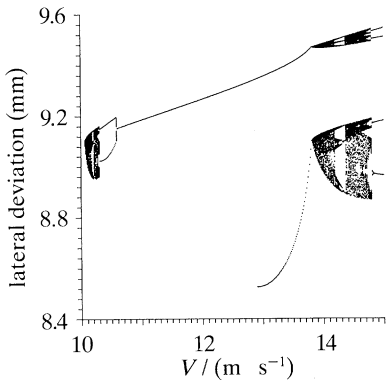


Figure 4

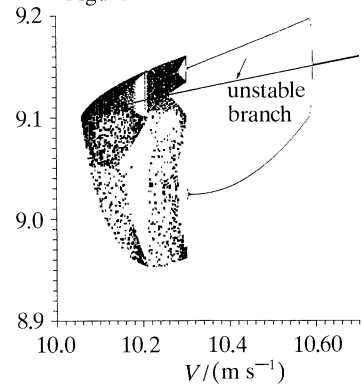


Figure 3. Bifurcation diagram for the wheelset. Only stable solutions are shown.

Figure 4. Part of figure 3. Bifurcation diagram for the wheelset. The arrow points at the unstable periodic solution branch, which is mentioned in the text.

PATH determines the solutions with a relative error of $10^{-9}$. When we investigate chaos, we let the integration in time continue until we are convinced, that the small transients have died out. Then we start to construct the Poincaré section or amplitude plot for that particular speed.

## 5. The results

In this section we describe the dynamical behaviour of the wheelset in the speed range $0 < V < 50$ m s$^{-1}$, which corresponds to 0–180 km h$^{-1}$.

At low speeds the trivial solution of our dynamical system is asymptotically stable. The trivial solution corresponds to a stable rolling of the wheelset along the centreline of the track.

When the speed grows, a supercritical Hopf bifurcation will be reached at $V = 10.050$ m s$^{-1}$. The steady solution loses stability at that speed, and it remains unstable for all speeds up to the maximum speed, we have investigated. The bifurcating periodic solution has a period of 1.64 s, it is asymptotically stable and its amplitude grows very fast with the speed. At $V = 10.056$ m s$^{-1}$ the amplitude of the oscillation is so large, that the flange hits the rail, and at still higher speeds the wheelset will move chaotically. This chaotic behaviour has recently been found by Meijaard (1991) in another wheelset model. The bifurcation diagram on figure 3 illustrates the dynamics of the wheelset up to $V = 15$ m s$^{-1}$. Figure 4 is an enlarged picture of the chaotic range and the bifurcations up to $V = 10.7$ m s$^{-1}$. It is seen that no periodic windows exist. The chaotic attractor contracts near $V = 10.2$ m s$^{-1}$ onto three bands, which grow narrower with growing speed. The central band converges towards the flange contact point 0.0091 m from the left side. When this point is reached at $V$ approximately equal to 10.21 m s$^{-1}$, the chaotic attractor explodes. At still higher speeds the chaos concentrates onto four narrow bands which represent two asymmetric oscillations with double period. These modes go through a reverse period doubling at $V = 10.32$ m s$^{-1}$. The period doubling is verified by a calculation of the Floquet multipliers. When we approach $V = 10.32$ m s$^{-1}$ from the right following the phase-parameter space path a Floquet multiplier leaves the unit disc through $-1$ at $V = 10.32$ m s$^{-1}$. In this context please remember that the negative




PHILOSOPHICAL TRANSACTIONS OF THE ROYAL SOCIETY A MATHEMATICAL, PHYSICAL & ENGINEERING SCIENCES

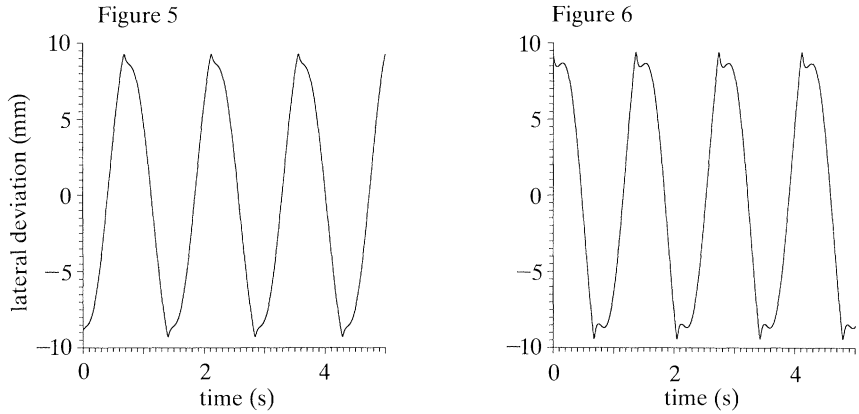


Figure 5. Lateral oscillation against time at $V = 12.0$ m s$^{-1}$.

Figure 6. Lateral oscillation against time at $V = 13.5$ m s$^{-1}$.

displacements are missing on the diagram. We see only the maximum value of each of the two different modes. Both modes oscillate around its own off-centre neutral line with a mean yaw different from zero. Their basins of attraction are separated by the inset of an unstable, symmetric oscillation, which is also shown on figure 4. The path of the unstable, symmetric oscillation enters the gap which separates the chaotic symmetric solutions from the asymmetric ones, right in the middle. The unstable solution can be traced deeply into the chaotic region from right to left.

At $V = 10.59$ m s$^{-1}$ the asymmetric solutions have flange contact at both rails. Below that speed the flange only touches either the left or the right rail during one period of oscillation. $V = 10.59$ m s$^{-1}$ is a bifurcation point, where the symmetric oscillation becomes asymptotically stable in a 'reverse symmetry breaking'. We find that a Floquet multiplier enters the unit disc through $+1$, when $V$ decreases through 10.59 m s$^{-1}$.

Figure 5 shows a short time series of the oscillation at $V = 12$ m s$^{-1}$. One observes the development of two new local extrema within one period, and figure 6 shows these fully developed extrema. On figure 3 the lower curve indicates the development of these new extrema as a function of $V$.

At $V = 13.81$ m s$^{-1}$ these new extrema have grown to a value, where another flange contact occurs at each of the rails during one period. A Floquet multiplier tends towards $-1$, when $V$ grows towards 13.81 m s$^{-1}$. Figure 7 shows a blow up of the bifurcation at the lower curve of figure 3 for $V = 13.81$ m s$^{-1}$, where chaos develops.

Figure 8 shows the bifurcations for $14.10$ m s$^{-1} < V < 14.90$ m s$^{-1}$. When $V$ decreases through 14.33 m s$^{-1}$, a Floquet multiplier leaves the unit disc through $+1$. The asymmetric solution with three positive plus two negative maxima and fundamental period then changes into two, asymmetric solutions, which turn chaotic for decreasing $V$. Notice again the flange contacts during one full period. The points are marked with arrows on figure 8.

When $V$ grows through 14.38, a Floquet multiplier goes through $+1$. We again have flange contact and a broad band of chaos develops.

The right-most bifurcation point on figure 8 is at $V = 14.83$ m s$^{-1}$. To the right of 14.83 we see two asymmetric oscillations; each of them with two maxima within one period. When $V$ decreases through 14.83 m s$^{-1}$, a Floquet multiplier leaves the unit

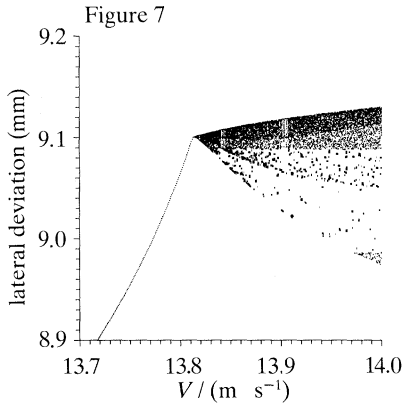


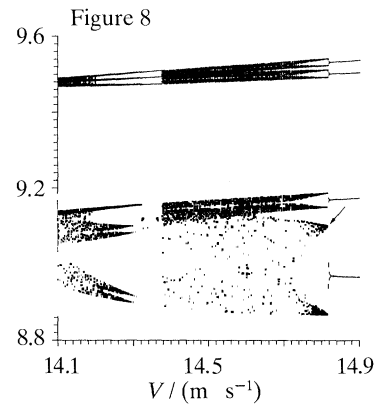


Figure 7. Enlarged part of figure 3 with the bifurcation to chaos at $V = 13.81$ m s$^{-1}$.

Figure 8. Bifurcation diagram for the wheelset. Only stable solutions are shown. The disjoint parts of the diagram represent different maxima of one and the same oscillation within one period. The arrows mark points of flange contact.

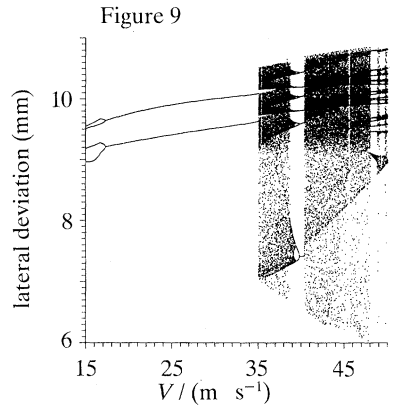


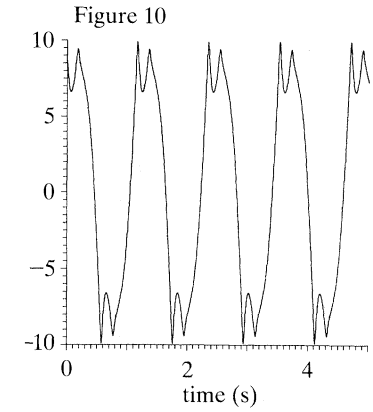


Figure 9. Bifurcation diagram for the wheelset. To the left two stable asymmetric oscillations are found; each with two maxima per period. In the middle one stable symmetric oscillation is found with two maxima per period. To the right chaos is found with periodic windows.

Figure 10. Lateral oscillation against time. $V = 25.0$ m s$^{-1}$.

disc through $-1$, and a period doubling takes place. The maximum on the lowest branch grows very fast with decreasing $V$, and when the flange hits the rail during that part of the cycle, chaos immediately develops.

Figure 9 illustrates the behaviour in the range $15 \text{ m s}^{-1} < V < 50 \text{ m s}^{-1}$. When $V$ grows through $17.23 \text{ m s}^{-1}$, the two asymmetric solutions undergo a 'reverse symmetry breaking', and a new symmetric oscillation with two maxima develops. Figure 10 shows a short time series of the oscillation of the wheelset at $V = 25 \text{ m s}^{-1}$. The symmetric oscillation of the wheelset 'bangs' between the rails with two consecutive flange contacts at each rail before the wheelset moves over to flange contact with the other rail.

This symmetric oscillation exists, and it is asymptotically stable up to $V = 35.20 \text{ m s}^{-1}$. When $V$ grows through $35.20 \text{ m s}^{-1}$ one Floquet multiplier leaves the unit disc through $+1$. Broad band chaos is seen to develop explosively on figure 9, and we believe that the bifurcation to chaos is through intermittency. As an evidence

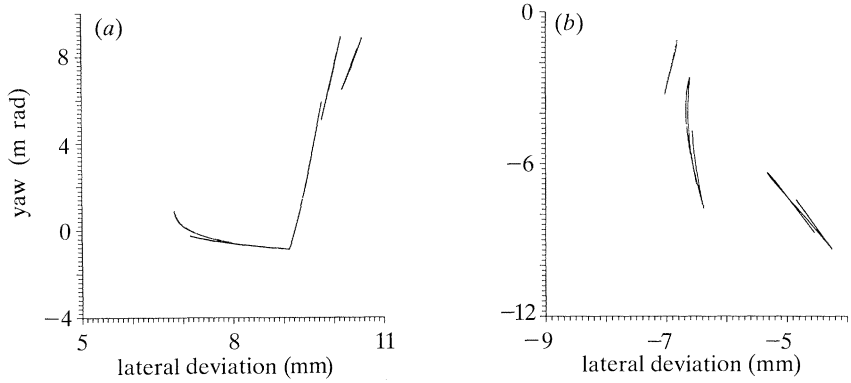


Figure 11. A projection of a Poincaré section for a chaotic solution at $V = 37.0$ m s$^{-1}$. (*a*) Shows the upper part and (*b*) the lower part of the section. Notice the asymmetry and the kink at $9.1 \times 10^{-3}$ m. The section is defined by $x_2 = 0$.

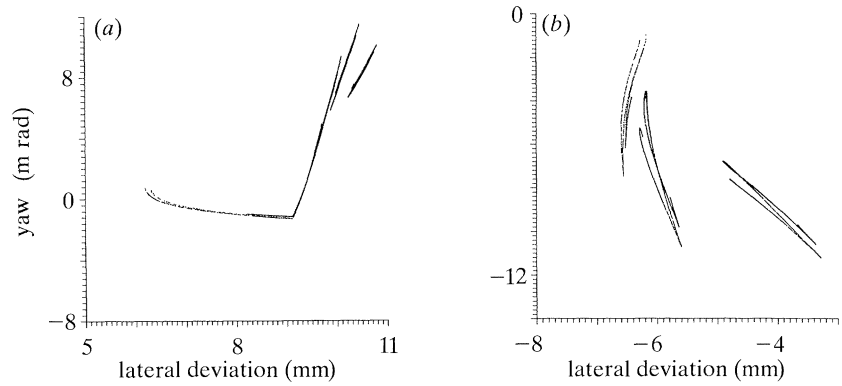


Figure 12. The same as figure 11 except for the speed $V$, which is now 45.0 m s$^{-1}$.

of the chaotic motion in the speed range 35.20 m s$^{-1}$ < $V$ < 38.5 m s$^{-1}$ we present a Poincaré section for $V = 37$ m s$^{-1}$ on figure 11. Figure 11*a* shows the upper part of the section and 11*b* the lower part. The layered structure does not appear clearly with this resolution, but the disconnected stripes are typical of chaotic motion.

The periodic window around $V = 40$ m s$^{-1}$ contains a symmetric solution with three maxima. When the speed decreases from 40 through $V = 39.78$ m s$^{-1}$, a Floquet multiplier leaves the unit disc through $-1$ and a period doubling sequence starts. With decreasing speed the chaos finally develops, which we have already described.

When the speed increases from 40 through 40.58 m s$^{-1}$, a Floquet multiplier leaves the unit disc through $+1$ and chaos develops explosively. The bifurcation is similar to the bifurcation at $V = 35.20$ m s$^{-1}$, and again we believe, that the bifurcation to chaos happens through intermittency.

On figure 12 we show a Poincaré section at $V = 45.0$ m s$^{-1}$. Figure 12*a* shows the upper and 12*b* the lower part of the section. Figure 12 is similar to figure 11, but the stripes are thicker and longer on figure 12 reflecting the more violent chaotic motion, which could be expected at the higher velocity, where more energy will be fed into the disturbance. Notice the asymmetry on figures 11 and 12 and the kink in the attractor at the lateral deviation 0.0091 m. The kink lies exactly where the wheel flange contacts the rail. The asymmetry of the chaotic attractors can be considered

Figure 13

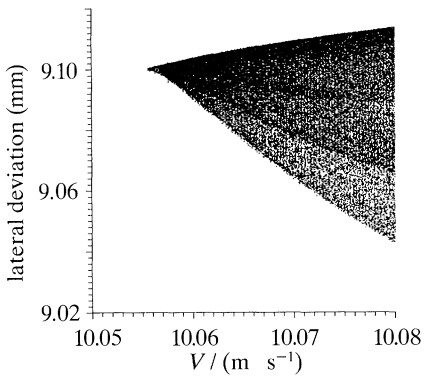


Figure 14

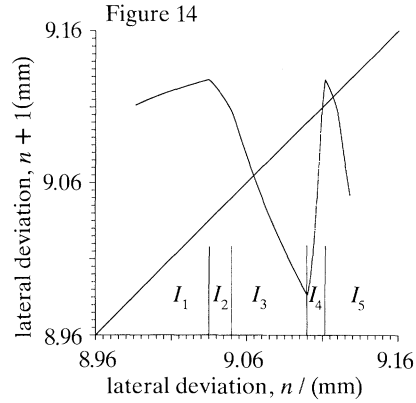


Figure 13. An enlarged part of figure 3. It shows the development of chaos without periodic windows for $10.05\ \mathrm{m\ s^{-1}} < V < 10.08\ \mathrm{m\ s^{-1}}$.

Figure 14. A 'first return map' for $x_1$. $V = 10.125\ \mathrm{m\ s^{-1}}$.

a common feature of chaotic behaviour in rail vehicle dynamics. It was noticed earlier by True (1989), G. Sauvage & J. P. Pascal (personal communication) and Knudsen *et al.* (1991).

At the end of the speed range, when $V$ tends towards $50\ \mathrm{m\ s^{-1}}$ the chaos concentrates onto narrow bands, but a well-defined subharmonic solution does not appear.

## 6. Investigation of chaotic behaviour by symbolic dynamics

Figure 13 shows an enlarged portion of the left part of figure 4. We see chaotic behaviour in the speed interval $10.056\ \mathrm{m\ s^{-1}} < V < 10.080\ \mathrm{m\ s^{-1}}$ without periodic windows. The lack of periodic windows makes it possible to extend the investigation of chaotic behaviour at a given speed to a whole range. We have examined several Poincaré sections in the speed interval $10.075\ \mathrm{m\ s^{-1}} < V < 10.175\ \mathrm{m\ s^{-1}}$. They all share the same qualitative structure, and they will therefore not be shown here.

Instead we show on figure 14 a first return map at the speed $V = 10.125\ \mathrm{m\ s^{-1}}$. We have plotted the value of $x_1$ in the $n$ plus first intersection with our Poincaré section against its value in the $n$th intersection.

The structure of the points constituting the first return map is remarkably close to a one-dimensional curve. We have examined several first return maps in the speed interval, and they are all very similar. Therefore we chose to show only one of them.

The $n$ axis can be divided into five intervals, which are characterized by the number and sequence of flange contacts in one full return map. They are numbered $I_1$ to $I_5$ on figure 14. $I_1$ contains the points, which describe a motion with flange contact only at its maximum, when the trajectory returns to the Poincaré section. The points in $I_2$ have an additional flange contact at the minimum of $x_1$. The points in $I_3$ characterize a motion that starts without flange contact; there is flange contact at the minimum of $x_1$ but none when the trajectory returns to the Poincaré section. The points in $I_4$ start with flange contact; there is another flange contact at the minimum of $x_1$, and there may or may not be flange contact, when the trajectory returns to the Poincaré section. Finally, $I_5$ contains the points of a motion, which initially has flange contact, has no flange contact at the minimum of $x_1$, and may or may not have flange contact, when it returns to the maximum value. As the speed




PHILOSOPHICAL TRANSACTIONS OF THE ROYAL SOCIETY A MATHEMATICAL, PHYSICAL & ENGINEERING SCIENCES

is decreased through approximately 10.107 m $s^{-1}$, a qualitative change occurs, in that the points in $I_1$ may or may not have flange contact when the trajectory returns to the Poincaré section.

The shape of the first return map suggests an investigation of the chaotic behaviour by the method of symbolic dynamics. We shall therefore define and investigate a one-dimensional iterated map on an interval, $f: I \to I$, where $I = \bigcup_{i=1}^{5} I_i$. $f$ is assumed to be continuous everywhere and differentiable everywhere except on the boundaries between the subintervals.

We require that $f$ maps the five intervals onto each other in the following way:

$$f(I_1) \supset I_5, \quad f(I_2) \supset I_4 \cup I_5, \quad f(I_3) \supset I_1 \cup I_2 \cup I_3, \quad f(I_4) \supset I, \quad f(I_5) \supset I_3 \cup I_4 \cup I_5.$$

We impose the following restrictions on the derivative of $f$: $0 < a < f'(I_1)$; $0 < b < -f'(I_2)$; $1 < c < -f'(I_3)$; $1 < d < f'(I_4)$ and $1 < e < -f'(I_5)$. All the constants $a, \ldots, e$ are assumed to be positive. We add the additional constraints: $aec > 1$, $aed > 1$, $aee > 1$, $bd > 1$ and $eb > 1$.

We would like to show that $f$ is chaotic on $I$. First, we show that $I$ contains an attracting set, which is in fact $I$ itself. From the definition of $f$ we easily see that $I$ is an attracting set since $\bigcap_{k=1}^{\infty} f^k(I) = I$. Second, we show that $I$ is a strange attractor for $f$. To achieve that we must show (i) that $f$ exhibits sensitive dependence on initial conditions in all of $I$, and (ii) that $I$ is topologically transitive under $f$.

*ad* (i) $f$ has a derivative with modulus less than one only in the intervals $I_1$ and $I_2$. Let us consider first an orbit passing through $I_1$. This orbit will first enter $I_5$ and next enter either $I_3$, $I_4$ or $I_5$. Then either $|(f^3)'(I_1)| > aee > 1$, or $> aec > 1$ or $> aed > 1$. Next we consider an orbit passing through $I_2$. When $x \in I_2$, then $f(x) \in I_4 \cup I_5$, but then $|(f^2)'(I_2)| > bd > 1$ or $> eb > 1$. Thus $f$ will expand intervals and therefore exhibits sensitive dependence on the initial conditions.

*ad* (ii) From (i) it follows, that for any subset $U \subset I$ there exists a positive integer $n$, such that $f^n(U) \supset I$, and therefore $I$ is topologically transitive under $f$. Combining (i) and (ii) we have proven that $I$ is a strange attractor for $f$.

Up to here we only have shown the existence of a strange – or chaotic – attractor, but we know nothing about its global structure yet.

Let us extend our analysis to the global structure of all periodic and non-periodic orbits by applying symbolic dynamics on five symbols, each corresponding to one of the five subintervals of $I$. We define the itinerary of a point $x \in I$ as the infinite symbol sequence $S(x) = s = s_0 s_1 s_2 s_3 \ldots$, where $s_k$ is 1 if $f^k(x) \in I_1$, and similarly for the other four subintervals. It is clear that for any point $x$ there exist one and only one itinerary. Please note that the six boundary points make up a five-cycle. We therefore know the future of all six boundary points under $f$, so we are not concerned with these points in the following.

The possible itineraries are given by the transition matrix $A$ (Wiggins 1988, pp. 102–103), which is

$$A = \begin{pmatrix} 0 & 0 & 0 & 0 & 1 \\ 0 & 0 & 0 & 1 & 1 \\ 1 & 1 & 1 & 0 & 0 \\ 1 & 1 & 1 & 1 & 1 \\ 0 & 0 & 1 & 1 & 1 \end{pmatrix}.$$

The transition matrix $A$ contains a 1 for the transition $(i, j)$ if $f(I_i) \supset I_j$, and a 0 otherwise. An itinerary is allowed if for all transitions $s_i s_{i+1}$ the transition matrix

contains a 1, $(A)_{s_i s_{i+1}} = 1$. The set of all possible itineraries are called $\Sigma_A$, and it is possible to verify that $f$ on $I$ is topologically conjugate to $\sigma_A$, where $\sigma_A$ is the subshift of finite type (Wiggins 1988, pp. 101–108). We can therefore describe the dynamics of $f$ on $I$ by considering the dynamics of $\sigma_A$ on $\Sigma_A$. Note that the transition matrix reveals that there exist a subset of $I_4 \cup I_5$ where the dynamics of $f$ are chaotic on a Cantor set, which is topologically conjugate to the full shift on two symbols, with all sequences allowed. The existence of this set is caused by the unstable fixed point in $I_4$, which has a non-degenerate homoclinic orbit in $I_4 \cup I_5$.

We next define a metric $d$ on $\Sigma_A$ by

$$d(s, \bar{s}) = \sum_{i=0}^{\infty} 2^{-i} \frac{|s_i - \bar{s}_i|}{1 + |s_i - \bar{s}_i|}.$$

It can easily be verified that if $d(s, \bar{s}) < 1/2^{M+1}$ then $s_i = \bar{s}_i$, $i \leqslant M$, and if $s_i = \bar{s}_i$, $i \leqslant M$ then $d(s, \bar{s}) \leqslant 1/2^M$.

We want to prove the following.

**Theorem.** *$f$ on $I$ is topologically conjugate with $\sigma_A$ on $\Sigma_A$ under the homeomorphism $S$.*

*Proof.* We must show that $S: I \to \Sigma_A$ is a homeomorphism.

$S$ is one-to-one. For any $x \neq y$ in $I$, there exists a positive integer $n$, such that $f^n(x)$ and $f^n(y)$ belong to different intervals, because $f$ expands intervals.

$S$ is onto. For any symbolic sequence $s$, allowed by the transition matrix $A$ there exists exactly one point $x \in I$, such that $S(x) = s$, since $f$ expands intervals.

$S$ is continuous. Given $\epsilon > 0$, we consider an arbitrary $x \in I$. First we pick a positive integer $n$ such that $\epsilon > 2^{-(n+1)}$. Since $x$ is not a boundary point then, by continuity of $f$, there exist a neighbourhood $U$ of $x$, such that for any $y \in U$, $d(S(x), S(y)) < \epsilon$. From $x$ and $U$ we can now choose a $\delta > 0$, such that the relation $\forall \epsilon > 0 \, \exists \delta > 0 \, |x - y| < \delta \Rightarrow d(S(x), S(y)) < \epsilon$ holds.

$S^{-1}$ is continuous. Given $s = s_0 s_1 s_2, \ldots, s_n, \ldots, \in \Sigma_A, x = S^{-1}(s)$ is not a boundary point. Because of continuity of $f$, then for a given $\epsilon > 0$, we can find a neighbourhood $U$ of $x$, such that $S(U) = s_0 s_1 \ldots s_n *$, where $*$ is any infinite symbolic sequence such that the entire sequence is allowed by the transition matrix $A$. We can now choose a $\delta < 1/2^n$, such that for $y \in U$ then $d(S(y), s) < \delta \Rightarrow |x - y| < \epsilon$.

Thus we have shown that $S$ is a homeomorphism. It is easy to see that $S(f) = \sigma_A(S)$ holds. QED.

Having showed the topological conjugacy between $f$ and $\sigma_A$, we are now in a position to make statements about the global structure of orbits for $f$ by considering the much simpler function $\sigma_A$.

It can be shown that the number of points $x$, for which $f^k(x) = x$, for some positive integer $k$, is the trace of the transion matrix to the power $k$. The number of periodic orbits of prime period $k$, $N(k)$, can then be calculated by

$$N(k) = (\mathrm{tr}\,(A^k) - \sum_{1 \leqslant i < k;\, i \mid k} N(i) \cdot i)/k,$$

where tr denotes the trace, and $i \mid k$ means '$i$ divide $k$'. From $A$ it can be shown that the trace of $A$ to the power $k$ can be expressed recursively as

$$\mathrm{tr}\,(A^k) = 3\mathrm{tr}\,(A^{k-1}) - \mathrm{tr}\,(A^{k-2}) + 3\mathrm{tr}\,(A^{k-3}) - \mathrm{tr}\,(A^{k-4}), \quad k > 4.$$

Table 2

| $k$ | $\mathrm{tr}\,(A^k)$ | $N(k)$ | $k$ | $\mathrm{tr}\,(A^k)$ | $N(k)$ |
|---|---|---|---|---|---|
| 1 | 3 | 3 | 11 | 156027 | 14184 |
| 2 | 7 | 2 | 12 | 462703 | 38496 |
| 3 | 27 | 8 | 13 | 1372179 | 105552 |
| 4 | 79 | 18 | 14 | 4069303 | 290520 |
| 5 | 228 | 45 | 15 | 12067812 | 804504 |
| 6 | 679 | 108 | 16 | 35787967 | 2236374 |
| 7 | 2019 | 288 | 17 | 106131819 | 6243048 |
| 8 | 5983 | 738 | 18 | 314741623 | 17484624 |
| 9 | 17739 | 1968 | 19 | 933389139 | 49125744 |
| 10 | 52612 | 5238 | 20 | 2768033284 | 138399030 |

This recursive formula for the trace can be solved analytically and the solution is

$$\mathrm{tr}\,(A^k) = 2\cos\left(k\left(\pi + \arctan\left(\frac{\sqrt{(6(\sqrt{13}-1))}}{3-\sqrt{13}}\right)\right)\right)$$
$$+(\tfrac{1}{4}(3+\sqrt{13}+\sqrt{(6(1+\sqrt{13}))}))^k + (\tfrac{1}{4}(3+\sqrt{13}-\sqrt{(6(1+\sqrt{13}))}))^k.$$

Note that for large $k$ the second term dominates. Table 2 shows the trace and number of prime periodic orbits for $k$ up to 20. An analytic expression for the topological entropy can also be given:

$$h = \log(\tfrac{1}{4}(3+\sqrt{13}+\sqrt{(6(1+\sqrt{13}))})).$$

## 7. Conclusions

The results presented here help us to understand the complicated behaviour of a rolling wheelset in its dependence on its speed. Very soon after the supercritical Hopf bifurcation, where the trivial solution loses its stability, the first chaotic speed interval appears. With growing speed the chaos alternates with periodic symmetric or asymmetric solutions. It is very interesting to notice the dominance of asymmetry in the chaotic as well as in the periodic behaviour. The asymmetric oscillations will, if they persist over longer distances, be the cause of lopsided wear of the wheelset. When a wheelset gets unsymmetric the trivial solution becomes unstable for lower speeds, so the wheelset will run more in the asymmetric modes than it did before and the result is an amplification of the hunting motion.

Lopsided wear has been observed on several occasions, where simple explanations were found. We are, however, left with many cases that can only be satisfactorily explained by assuming that the wheelset has oscillated asymmetrically.

The results also demonstrate that chaotic behaviour, as such, is no more dangerous or undesirable than violent periodic motion.

We have only examined one set of characteristic parameter values for the wheelset. To help the engineers improve the dynamics of the wheelset the effects of the change of the other parameters on the dynamics of the wheelset must be examined. The most important parameters are the wheel and rail geometries, the coefficient of adhesion, the axle load and the spring stiffness; here a torsional spring and damper should be added to the suspension. We shall continue our investigations along these lines with the main emphasis on realistic wheel and rail profiles and stiffer spring.




PHILOSOPHICAL TRANSACTIONS OF THE ROYAL SOCIETY A MATHEMATICAL, PHYSICAL & ENGINEERING SCIENCES

Finally, we emphasize that our symbolic dynamics calculations show that the phenomenon of chaos in the model is structurally stable.

A part of this work (H.T.) was supported by the Danish Council for Scientific and Industrial Research, grant no. 16-4786.M.

## References

Cooperrider, N. K. 1972 The hunting behaviour of conventional railway trucks. *ASME J. Engng Industry* **94**, 752–762.

De Pater, A. D. 1960 The approximate determination of the hunting movement of a railway vehicle by aid of the method of Krylov and Bogoljubow. In *Proc. 10th Int. Congr. of Applied Mechanics,* Stresa. *Appl. Sci. Res.* A **10**.

Enright, W. H., Jackson, K. R., Nørsett, S. P. & Thomsen, P. G. 1986 Interpolants for Runge–Kutta formulas. *ACM Trans. Math. Software* **12**, 193–218.

Guckenheimer, J. & Holmes, P. 1983 *Nonlinear oscillations, dynamical systems and bifurcations of vector fields.* New York, Berlin, Heidelberg and Tokyo: Springer-Verlag.

Huilgol, R. R. 1978 Hopf-Friedrichs bifurcation and the hunting of a railway axle. *Q. Jl appl. Math.* **36**, 85–94.

Jaschinski, A. 1990 On the application of similarity laws to a scaled railway bogie model. Ph.D. thesis, Technical University Delft, The Netherlands.

Kaas-Petersen, C. 1986*a* Chaos in a railway bogie. *Acta Mechanika.* **61**, 89–107.

Kaas-Petersen, C. 1986*b*, 1989 PATH user's guide. Technical University of Denmark, Laboratory of Applied Mathematical Physics.

Kalker, J. J. 1990 *Three-dimensional elastic bodies in rolling contact.* Dordrecht: Kluwer Academic Publishers.

Kisilowski, J. & Knothe, K. (eds) 1991 *Advanced railway vehicle system dynamics.* Warszawa: Wydawnictwa Naukowo-Techniczne.

Klingel, W. 1883 Über den Lauf der Eisenbahnwagen auf gerader Bahn. Organ für die Fortschritte des Eisenbahnwesens in technischer Beziehung. *Neue Folge* XX, **4**, 113–123 & *Tafel* XXI.

Knudsen, C., Feldberg, R. & Jaschinski, A. 1991 Nonlinear dynamic phenomena in the behaviour of a railway wheelset model. *Nonlinear Dynamics* **2**, 389–404.

Matsudeira, T. 1960 Paper awarded prize in the competition sponsored by the Office of Research and Experiment of the International Union of Railways. Utrecht.

Meijaard, J. P. & De Pater, A. D. 1989 Railway vehicle system dynamics and chaotic vibrations. *Int. J. Nonlinear Mech.* **24**, 1–17.

Meijaard, J. P. 1991 Dynamics of mechanical systems. Ph.D. thesis, Technical University Delft, The Netherlands.

Petzold, L. 1983 Automatic selection of methods for solving stiff and nonstiff systems of ordinary differential equations. *SIAM J. Sci. Stat. Comput.* **4**, 136–148.

Thompson, J. M. T. & Stewart, H. B. 1986 *Nonlinear dynamics and chaos*, pp. 51–290. Chichester, New York, Brisbane, Toronto & Singapore: John Wiley and Sons.

True, H. 1989 Chaotic motion of railway vehicles. In *Proc. 11th IAVSD Symp. on Vehicle systems dynamics in the dynamics of vehicles on roads and on tracks* (ed. R. Anderson), pp. 578–587. Amsterdam/Lisse: Swets & Zeitlinger.

Vermeulen, P. J. & Johnson, K. L. 1964 Contact of nonspherical elastic bodies transmitting tangential forces. *J. appl. Mech.* **31**, 338–340.

Wickens, A. H. 1965 The dynamic stability of railway vehicle wheelsets and bogies having profiled wheels. *Int. J. Solids Structures* **1**, 319–341.

Wiggins, S. 1988 *Global bifurcations and chaos.* New York, Berlin, Heidelberg and Tokyo: Springer-Verlag.





PHILOSOPHICAL TRANSACTIONS OF THE ROYAL SOCIETY A MATHEMATICAL, PHYSICAL & ENGINEERING SCIENCES